Demodulation Technique for Broken Rotor Bar Detection in Inverter-fed Induction Motor under non-stationary Conditions

Tomas A. Garcia-Calva, *Student Member IEEE*, Daniel Morinigo-Sotelo, *Member, IEEE*, Arturo Garcia-Perez, *Member, IEEE*, David Camarena-Martinez and Rene de J. Romero-Troncoso, *Senior Member, IEEE*

left

***Abstract*--Transient motor current signature analysis has become a mature technique for fault detection in induction motors. By using start-up transients, the whole range of slip in the machine is exploited to generate well-defined fault frequency patterns. However, in the inverter-fed motor case, the fault-patterns is always close to the supply frequency and often of low amplitude. Therefore, it is difficult to distinguish and localize the fault-patterns. In this paper, a novel method is proposed to create a new fault-pattern; the proposed technique can concentrate the fault-harmonic in a specific frequency bandwidth and avoid the spectral leakage by reducing the supply frequency amplitude. The methodology has been validated through experimental tests carried out to detect broken rotor bar in an induction motor started through a voltage source inverter.**

***Index Terms*—Condition monitoring, fault diagnosis, induction motors, signal processing, spectral analysis, stator current analysis.**

I. Introduction

INDUCTION motors (IMs) are widely used in industry due to their excellent performance and high-robustness [1]. However, these electrical machines are susceptible to several types of faults. It has been demonstrated that every fault introduces an additional frequency component in the stator current [2]-[3]. Broken rotor bar (BRB) is one of the most difficult fault to detect since the additional frequency component appears too close to the supply frequency. Several methods have been used to detect BRB faults in IMs [4]-[5]. Most of the works still deal with line-fed IMs and under stationary conditions. Recently, it is more common to see IMs fed by voltage source inverters (VSI) [6]. Furthermore, stationary operation is quite unusual in the industrial environment due to the existence of voltage variations, speed oscillations, and load changes; consequently, the detection of faults must be approached under non-stationary conditions.

In this context, some researchers have developed techniques allowing fault analysis under transient conditions [7]. For instance, in [8] the authors proposed to use an adaptive time-frequency (t-f) transform. This proposed strategy is based on the correlation between the stator current signal and a family of pre-defined t-f atoms. An application of multi-rate digital signal processing for diagnosing BRB can be found in [9]. The major contribution of the authors is the development of a resampling technique that allows separating the fault component from the variable supply frequency. In [10], a combination between the complete ensemble empirical mode decomposition and the multiple signal classification (MUSIC) algorithm is proposed. In this case, the proposed method allows decomposing the signal in different modes, which makes fault identification more accurate after removing the modes considered as noise. Another methodology using a reassignment technique for sharpening the t-f representation by relocating the data according to local estimates of instantaneous frequency and group delay was proposed in [11]. All the above-mentioned methods allow tracking the fault-related frequency in the t-f plane. However, these techniques have an important drawback since the energy of the fundamental supply frequency is still higher than the fault-related one; therefore, spectral leakage has an adverse impact.

Recently, some works have proposed the use of demodulation techniques to eliminate the fundamental supply frequency and to extract a reliable fault indicator based on stator currents measurements [12]-[14]. The application of a demodulation process shifts the stator current spectrum along the frequency domain in such a way that the fundamental component is sent to the zero value. Consequently, subtracting the average value from the demodulated signal eliminates the masking effect of the spectral leakage. Several authors have confirmed its usefulness for rotor asymmetries detection in IMs [15]-[17], and in generators [18]-[19]. However, these methods use the stator current signal and presume that the IM is line-fed and in stationary conditions.

The main contribution of this research is the proposal of a methodology based on an IM stator current non-uniform demodulation under non-stationary conditions that detects BRB faults. Although the demodulation technique is an effective method for the steady state, it has not been applied to non-stationary conditions yet. This concept of uniform

This work was supported in part by the Mexican Council of Science and Technology (CONACYT) by the scholarship 487058, México City, México.

T. A. García-Calva, A. García-Pérez and D. Camarena-Martínez, are with the Electronic Engineering Department, University of Guanajuato, Guanajuato, 36700, México (e-mails: ta.garciacalva@ugto.mx; arturo@ugto.mx; david.camarena@ugto.mx).

D. Moriñigo-Sotelo is with the Electrical Engineering Department, University of Valladolid, Valladolid 47002, Spain (e-mail: daniel.morinigo@eii.uva.es).

R. de J. Romero-Troncoso is with the Autonomous University of Querétaro, HSPdigital Research Group, Faculty of Engineering, San Juan del Río, 76806, México (e-mail: troncoso@hspdigital.org).

demodulation is extended to non-uniform demodulation for the non-stationary regime. This method isolates the fault-related frequency from the variable source frequency in an inverter-fed IM. The advantages of the proposed technique are its low computational complexity of the signal processing and its precise fault-related frequency detection.

II. Background

A. Broken Rotor Bar

The phase current of a healthy IM contains the fundamental component and its harmonics. The breaking of a rotor bar produces an amplitude modulation of the stator current. As a result, two additional frequencies known as left-side harmonic and right-side harmonic appear at ω_l=(1-2s)ω_s and ω_r=(1+2s)ω_s respectively [20]lthough, where ω_s is the main frequency, and s is the rotor slip. The equations of the three stator currents for a faulty IM can be written as follows:

$$i_a(t) = I_1\cos(\omega_s t) + I_l\cos(\omega_l t+\varphi_l) + I_r\cos(\omega_r t+\varphi_r)+\eta_a(t) \qquad (1)$$

$$i_b(t) = I_1\cos(\omega_s t - \tfrac{2\pi}{3}) + I_l\cos(\omega_l t - \tfrac{2\pi}{3}+\varphi_l) + I_r\cos(\omega_r t - \tfrac{2\pi}{3}+\varphi_r)+\eta_b(t) \qquad (2)$$

$$i_c(t) = I_1\cos(\omega t - \tfrac{4\pi}{3}) + I_l\cos(\omega_l t - \tfrac{4\pi}{3}+\varphi_l) + I_r\cos(\omega_r t - \tfrac{4\pi}{3}+\varphi_r)+\eta_c(t) \qquad (3)$$

where I_l corresponds to the amplitude of the fundamental components, I_l, I_{1r} are amplitudes of the fault frequencies, φ_l *and* φ_r are the phase angles, and η_a, η_b, η_c are independent noise signals due to the measurement system.

B. Sum of Adjacent Products

The sum of adjacent products (SAP) in an IM consists in the sum of the products of every two-adjacent phase currents, for a three-phase IM:

$$i_{sap}(t) = \begin{bmatrix} i_a & i_b & i_c \end{bmatrix} \cdot \begin{bmatrix} i_b \\ i_c \\ i_a \end{bmatrix} = i_a i_b + i_b i_c + i_c i_a \qquad (4)$$

The spectrum of i_{sap} is the result of two signal-processing procedures: amplitude demodulation and a superposition of sinusoids. In (4), the signal multiplication of two-phase currents in the time-domain involves double frequency shifting along the frequency-domain, one at the sum of the two original frequencies and one at their absolute difference expressed by

$$x(t)\cos(\omega_o t) \xleftrightarrow{FT} \tfrac{1}{2}\left[e^{j(\omega+\omega_o)}\right] + \tfrac{1}{2}\left[e^{j(\omega-\omega_o)}\right] \qquad (5)$$

After the calculation of every product, a superposition of sinusoids takes place when the addition is computed in (4). Precisely, a destructive interference effect is produced since fundamental components of demodulated signals differ in phase. Hence, the superposition operation suppresses the large amplitude of the demodulated fundamental and its harmonics.

Under ideal conditions, i.e. for a healthy three-phase IM, the calculation of (4) lead to:

$$i_{sap}(t) = -\tfrac{3}{4} I_1^2 \qquad (6)$$

It contains only a dc component, which can be easily suppressed by subtracting the average value in the time-domain. When a damage fault in the rotor bar occurs, the generated demodulation is not only by ω_s, but also by the sidebands ω_l and ω_r; thus, the application of the SAP method to the currents in the faulty IM gives

$$i_{sap}(t) = 3I_1(I_l+I_r)\cos(2s\omega_s t + \tfrac{2\pi}{3}) + 3I_l I_r\cos(4s\omega_s t + \tfrac{2\pi}{3}) - \tfrac{3}{4}I_1^2 - \tfrac{3}{4}I_l^2 - \tfrac{3}{4}I_r^2 \qquad (7)$$

It can be noticed that the application of the method results in three spectral components: a dc value, and two new fault terms located at $2s\omega_s$ and $4s\omega_s$. As the dc value can be easily removed, the theoretical components in i_{sap} related to BRB fault are the oscillating terms.

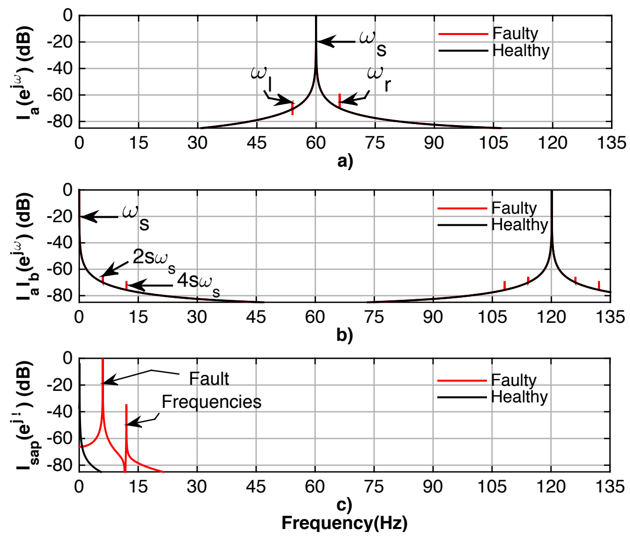

Fig. 1. Location of fault and fundamental components under stationary conditions. Spectra under healthy and faulty condition for: a) One phase current, b) Product of two phase-currents, and c) SAP method.

Fig. 1 shows the location of the frequency components of an IM under stationary analysis. First, the stator current spectra for a healthy and a faulty rotor are depicted in Fig. 1.a, where the ω_s and the fault components are too close to each other. Therefore, the amplitudes of ω_l and ω_r are affected by the spectral leakage of the fundamental component. Secondly, Fig. 1.b shows the demodulated current spectra of $I_a I_b(e^{j\omega})$ for the same healthy and faulty IM resulting from the product of two phase-currents. The demodulation process shifts the original spectrum to the left and the right by ω_s. Finally, the spectra of the signals obtained by the SAP method are shown in Fig. 1.c. The results show that the principal components are suppressed for the motor with healthy rotor, whereas for the faulty rotor in the spectrum $I_{sap}(e^{j\omega})$ the main components are the fault frequencies at $2s\omega_s$ and $4s\omega_s$. Waveforms simulation for stationary conditions in Fig.1 are presented assuming a line-fed IM at a constant supply 230V/60 Hz, with a constant angular speed of 3420 r.p.m. and slip of 0.05. Time domain signals were generated for 60.6815 seconds with a sampling frequency F_s=270 Hz. The peak values of the different frequency components of $i_a(t)$, $i_b(t)$ and $i_c(t)$ are: I=6.8 A, I_l=I_r=0.0054 A, and φ_l= φ_r =0.0. Spectra were obtained by applying the fast Fourier transform algorithm (2^{14} points) to the simulated sequences $i_a(t)$, $i_a(t)i_b(t)$ and $i_{sap}(t)$ to illustrate the prposed method.

C. Inverter-fed Induction Motor

When an inverter feeds the IM, voltage distortion is introduced and each component of the stator voltage produces a corresponding stator current component at the same frequency. In this case, the stator current for a faulty IM can be written as

$$i_\theta(t) = \sum_{h=0,1,3,..} I_h \cos(h\omega_s t + \varphi_\theta)$$
$$+ I_l \cos(\omega_l t + \varphi_l) + I_r \cos(\omega_r t + \varphi_r) \quad (8)$$

where θ is the current phase (θ=a,b,c), h is the harmonic order, and φ is the sinusoid phase. Applying the proposed method to (8), the resulting $i_{sap}(t)$ signal model is given by

$$i_{sap}(t) = \sigma_0 + \sigma_1 + \sigma_2 + \sigma_3 + \sigma_f \quad (9)$$

where

$$\sigma_0 = 3(I_0^2 + \frac{I_1^2}{2} + \frac{I_3^2}{2}) \quad (10)$$

$$\sigma_1(t) = 2I_0 I_1 \sum_{\theta=a,b,c} \cos(\omega_s t + \varphi_\theta) \quad (11)$$

$$\sigma_2(t) = \frac{I_1^2}{2} \sum_{\psi=\alpha,\beta,\gamma} \cos(2\omega_s t + \psi) \quad (12)$$

$$\sigma_3(t) = 2I_0 I_1 \sum_{\theta=a,b,c} \cos(3\omega_s t + \varphi_\theta) \quad (13)$$

and

$$\sigma_f(t) = 3I_1(I_l + I_r)\cos(2s\omega_s t + \varphi_f)$$
$$+ 3I_l I_r \cos(4s\omega_s t + 2\varphi_f) \quad (14)$$

where α=φ_a+φ_b, β= φ_b+φ_c, φ_f = φ_r-φ_l and γ= φ_c+φ_a.. When the phase-currents are exactly balanced (a=0, b=-2π/3, c=-4 π /3) the total current i_{sap} for a healthy motor is zero, whereas for a faulty motor the i_{sap} current contents two harmonic components independent of the superposition principle.

D. Short-time MUSIC Algorithm

Consider the multi-component signal $i_{sap}(t)$, based on signal model (9) it consists of a linear combination of (p=6) time-harmonics from the set

$$\left\{ e^{j\omega^h t} : \omega^h = (\omega_1^h, \ldots, \omega_D^h) \in \mathbb{R}^D, h = 1, \ldots, p \right\} \quad (15)$$

The multi-component signal model in the discrete-domain is expressed as:

$$i_{sap}[n] = \sum_{h=0}^{p-1} \sigma_i e^{2\pi j\omega^h n + \varphi_h} + \eta[n] \quad (16)$$

where $\eta[n]$ is a white Gaussian noise with zero mean and constant variance. The basic idea of MUSIC algorithm is to decompose $i_{sap}(t)$ into signal and noises subspaces. The task is to find out the frequency support $p = \{0\omega_s, 2s\omega_s, 4s\omega_s, \omega_s, 2\omega_s, 3\omega_s\}$ from a sequence $i_{sap}[n]$ sampled at $t = (n_1, \ldots, n_D)$, $0 \le n_d \le N_d$, $d = 1, \ldots, D$. It is possible to compute the time-frequency representation of the signal by sectioning $i_{sap}[n]$ into overlapping frames, multiplying the frames by a proper analysis window and applying the MUSIC algorithm of each frame as follows

$$Q_{MUSIC}[m,q] = \sum_{n=0}^{n=N_d-1} \frac{i_{sap}[n]w[n-ml]}{\sum_{k=p+1}^{o} \left| \mathbf{e}(\omega)^{*T} \mathbf{u}_k \right|^2} \quad (17)$$

where N_d is the length sequence, n is the discrete-time index, $w[n]$ is a rectangular analysis window, m is the position of the analysis window, l is the leap size between successive windows, o is the size of the eigenvectors, and q is the frequency index [21].

III. Simulation Results

A simulation scheme has been implemented in MATLAB by creating synthetic waveforms based on the voltage and current behavior of a VSI-fed IM. Synthetic waveforms were made by analyzing a soft transient starting. The duration of simulated data is 5 seconds for the transient state and 1 second for the stationary state. Mechanical rotor speed (n) in r.p.m. is given by:

$$n = \frac{120}{np}\omega_s(1-s) \quad (18)$$

where ω_s is the fundamental frequency of the input voltage in Hz, np is the number of poles, and s is the rotor slip, usually expressed in per-unit. Fig. 2, shows the slip variation between 1 and 0.02727 p.u. for a VSI started IM.

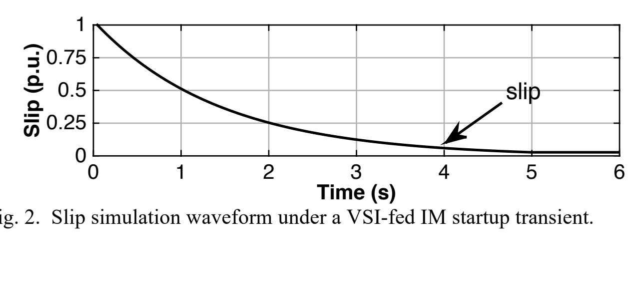

Fig. 2. Slip simulation waveform under a VSI-fed IM startup transient.

In time-varying conditions, such as startup transient the trajectory of fault-harmonics cannot be easily detected by conventional spectrum analysis, because $\omega_l(t)$ and $\omega_r(t)$ are spread across a wide frequency range; furthermore, they are close to the $\omega_s(t)$, making their correct observation difficult. In fact, fault-harmonics vary as a function of time according to the rotor slip and the supply frequency. The time-frequency content of one IM phase current during a startup transient is presented in Fig. 3. Fig. 3.a is related to a healthy rotor condition. The fundamental frequency increases linearly in time from 0 to 60 Hz. The first odd harmonics, $h_3(t)=3\omega_s(t)$ and $h_5(t)=5\omega_s(t)$, introduced by the VSI, are also present in the t-f plane. As mentioned in section 2, the bar breakage in the rotor produces the appearance of fault-harmonics at $\omega_l(t)$ and $\omega_r(t)$ in the frequency domain. Fig. 3.b shows their corresponding fault-trajectories, which evolve during the startup with positive slope and close to $\omega_s(t)$ in the t-f domain. Time-frequency profile of the harmonic content for the line current under startup transient is calculated by $i_a(t)$ = 60Hz/5sec t + 120Hz/5sec t + 180Hz/5sec t. When rotor is faulty, the faul-related harmonics are given by $(1\pm2s(t))\omega_s(t)$, where $\omega_s(t)$=60Hz/5sec t and the considered transient slip shown in Fig.2 is an exponentially decreasing slip function $s(t) = me^{nt} - 0.005$, with m=1.037 and n=-0.694.

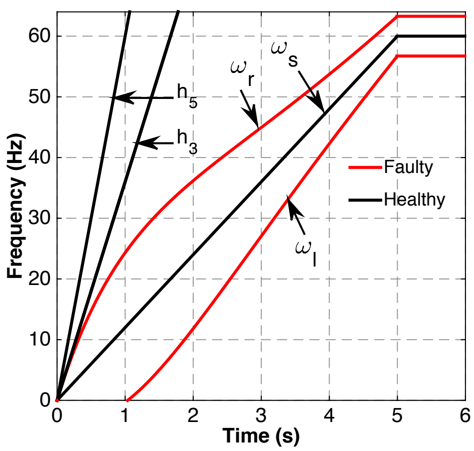

Fig. 3. Theoretical trajectories in VSI-fed IM startup. Conventional t-f analysis for: a) healthy rotor, and b) faulty rotor.

The theoretical trajectories of the harmonic content of the i_{sap} current of a healthy and faulty motor are shown in Fig. 4. As a consequence of the SAP method for a healthy induction motor, all the significant frequency components are canceled each other, hence i_{sap} contains only spectral residues (σ, σ_2, σ_3) located at ($\omega_s(t)$, $2\omega_s(t)$, $3\omega_s(t)$) as a result of (10)-(13). In contrast, when a rotor bar is broken a non-uniform demodulation produces a fault frequency component at $2s(t)\omega_s(t)$, which is spread in a frequency bandwidth proportional to the instantaneous slip and the instantaneous $\omega_s(t)$. A theoretical t-f analysis of the i_{sap} is depicted in Fig. 4.b, where a speed variation from 0 to 3502 r.p.m. in 5 seconds is considered. As can be seen, the most relevant harmonic evolution is the fault component; moreover, its trajectory is concentrated in a certain narrow frequency range band, leading to reliable fault detection.

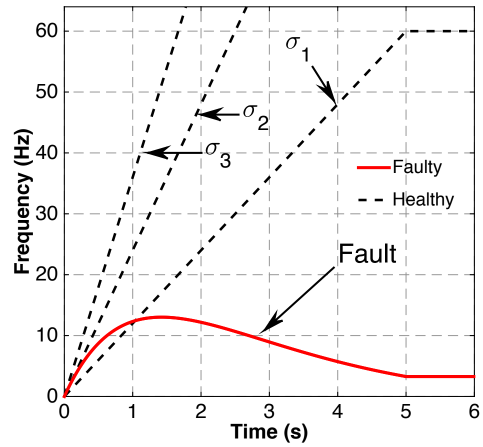

Fig. 4. Theoretical trajectories in VSI-fed IM startup of t-f analysis of the signal for: a) healthy rotor, and b) faulty rotor.

IV. Methodology

The proposed fault detection procedure includes the following processing stages:

1. First, a lowpass filter (LP) with cutoff frequency $\omega=\pi/D$ is used to band-limit the input signals; then the filtered signals are down-sampled by a factor D. This combined process is called decimation and limits the analysis in a frequency band (0 to F_s/D) where F_s is the sampling frequency. When the data acquisition system F_s is very high, it is necessary to consider a multi-stage decimation approach to reduce aliasing distortion [22].

2. The decimated signals are LP filtered once more to avoid the effect of spectral overlapping by demodulation. Now the time with cutoff frequency is $\omega=\omega_o$ and satisfies $\omega_o<\pi-\omega_o$ where ω_o is the maximum operating supply frequency and $\pi=F_s/2$. Then, the multiplication of every two adjacent phase IM currents is carried out.

3. Once the signals are band-limited and demodulated, the sum of the products sample per sample provides the value of the analysis sequence $i_{sap}[n]$.

4. The signal is windowed with a size of $w=130$ of samples to obtain a local spectrum by MUSIC algorithm. Finally, the window is sliding by every 3 samples along the complete sequence to compute the time-frequency decomposition. A simplified block diagram of the digital signal processing for the proposed method is illustrated in Fig. 5.

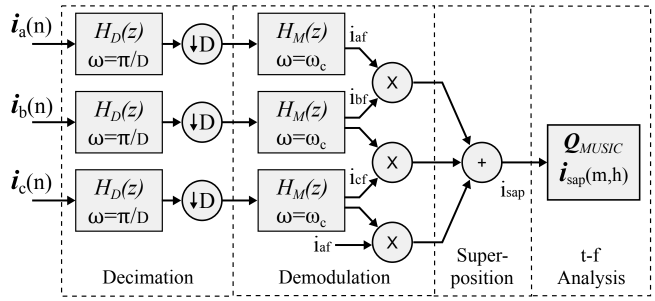

Fig. 5. Simplified block diagram representation of the proposed method.

V. Experimental Results

Experimental tests have been carried out to validate the presented approach. For this purpose, a three-phase IM (WEG model 00136APE48T) coupled to an alternator have been used. The parameters of the motor are presented in Table I.

TABLE I
Induction Motor Parameters

Rated power	kW	0.74
Poles	unit	2
Rotor bars	unit	28
Rated voltage	V	230/460
Rated current	A	2.9/1.4
Rated frequency	Hz	60
Rated speed	r.p.m.	3355
Efficiency	%	75.5
Power factor	p.u.	0.87
Rated torque	Nm	2.1

The experimental tests consist in using a soft startup controlled by a VSI (WEG model CFW08) to drive the IM.

The VSI drive uses pulse width modulation (PWM) technique and is programmed with a *v/f* (scalar) linear control. The *v/f* control principle adjusts a constant V/Hz ratio of the stator voltage by feed-forward control. It serves to maintain the magnetic flux in the IM at the desired level, which is adequate for applications like pumps, fan drives, belt conveyors, and others. The VSI parameters are reported in Table II.

TABLE II
Variable Source Inverter Parameters

Control method	V/F, PWM,16 bits
Commutation frequency	10 kHz
Rated output current at 220-240 V	7.0 A
Frequency limits	0-66 Hz
Automatic torque Boost	1.0%
Slip compensation	0.0%
DC link voltage regulation	380V

The programmed startup duration is 5 seconds and employs a linear frequency sweep from 0 to a selected operating frequency ω_o. The stator phase currents were sampled at 12.0 KHz. All signals were recorded for 6 seconds; 5s of startup and 1s of steady-state regime. Two cases were tested; the former is related to the VSI programmed with a conventional operating frequency ω_o=60 Hz and, the latter to the VSI programmed with a low ω_o=30 Hz. For both cases, healthy and faulty motor were analyzed. The faulty condition was created drilling a 2.0 mm diameter hole in the squirrel-cage bar. Fig. 6 shows the experimental setup. The fault diagnosis technique was implemented on a PC using Matlab software. The main limitation of broken rotor bar detection from a controlled VSI-fed motor is the closeness between supply frequency and the fault harmonics in the frequency domain. Since fundamental frequency amplitude is greater than the fault harmonics, the energy from the fundamental spectral line is spread into neighboring frequencies in the t-f domain. This difficult fault-harmonic detection even with high-resolution techniques. Time-frequency decomposition by short time MUSIC algorithm of the conventional current signal is depicted in Fig. 7.

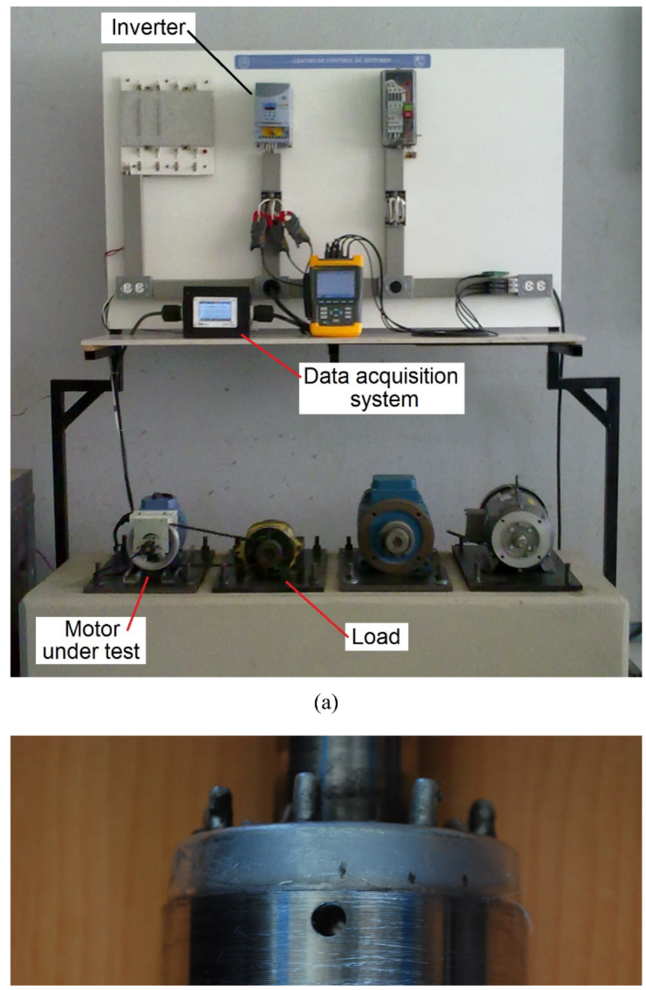

(a)

(b)

Fig. 6. Experimental set up: a) Motor test-bench. b) Faulty rotor with one broken bar.

Fig. 7 presents the t-f distribution of the line current for a healthy machine, where the principal component is $\omega_s(t)$ from 0 Hz to a maximum pre-programmed 60 Hz. Fig. 8 corresponds to the same machine with a faulty rotor.

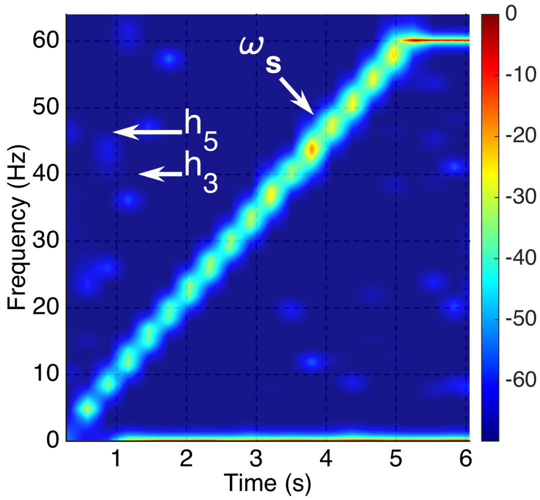

Fig. 7. Experimental result of inverter-fed IM startup (f_o=60 Hz). Time frequency distribution of one-phase current for the healthy motor.

The t-f distribution shows the fundamental component and the $\omega_l(t)$ harmonic, which apparently evolves parallel to the right and very close to $\omega_s(t)$.

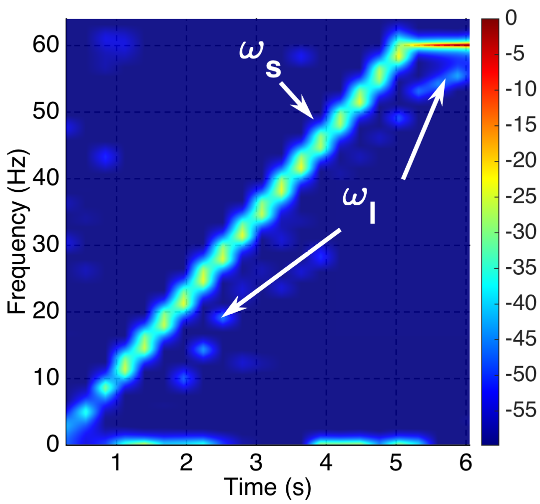

Fig. 8. Experimental result of inverter-fed IM startup (f_o=60 Hz). Time frequency distribution of one-phase current for the faulty motor.

Although the fundamental component and the left-side harmonic are perceptible during the startup transient, their trajectories in the time-frequency plane are very close to each other. This proximity makes it difficult to separate clearly their trajectories due to the important difference of energy between them, and therefore hindering their use for rotor condition monitoring purposes. It should be noted that since the energy of the fundamental frequency is much greater than the energy of the VSI harmonics, the evolution of harmonics h_3 and h_5 is not observable in the time-frequency representation. On the other hand, Fig. 9 and Fig. 10. illustrate the application of the proposed method and expose the clear difference between a healthy motor and a motor with a broken rotor bar. Fig. 9 provides the t-f distribution of i_{sap} for a healthy motor, where only two spectral components appear with small energy. One is the main component $\omega_s(t)$ mapped by the method to $\sigma_2(t)$ and the other is a dc component from a phase-current also mapped to $\sigma_1(t)$. Both $\sigma_1(t)$ and $\sigma_2(t)$ arise because of an unbalance between current-phases.

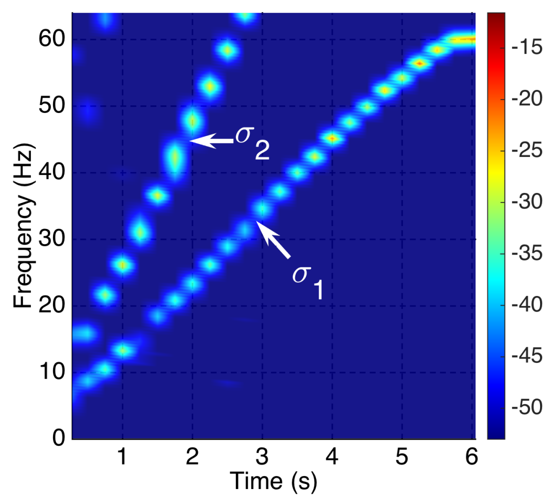

Fig. 9. Experimental result of inverter-fed IM startup (f_o=60 Hz). Time frequency distribution of i_{sap} current for the healthy motor.

Fig. 10 shows the same frequency components in a faulty condition analysis. However, the resulting t-f distribution of the faulty motor i_{sap} current reveals the presence of the broken bar related-harmonic $2s\omega_s(t)$, which is clearly observed especially during the transient start-up. The fault harmonic evolution drops in frequency after 5s due to the decrease of the slip as IM reach its steady state. The fault frequency $4s\omega_s(t)$ is not observed in Fig. 10 since the amplitude $3I(I_l+I_r)$ in (7) is much greater than $3I_lI_r$. In particular, comparing the fault frequencies $(1\text{-}2s(t))\omega_s(t)$ and $2s(t)\omega_s(t)$ in Fig. 8 and Fig. 10 respectively, it is clear that the method facilitates the identification of a damaged rotor.

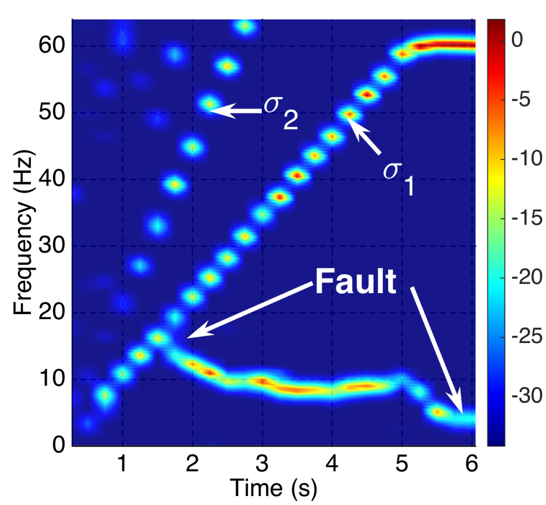

Fig. 10. Experimental result of inverter-fed IM startup (f_o=60 Hz). Time frequency distribution of i_{sap} current for the faulty motor.

An additional test starting the motor with a different operating frequency was made to verify the sensitivity of the approach against power supply frequency variations. The results in Fig. 11 illustrates that the frequency components have a similar behavior under a supply frequency sweep from 0 to 30 Hz.

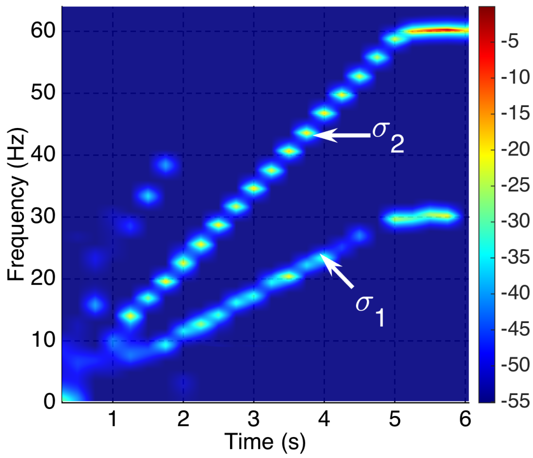

Fig. 11. Experimental result of inverter-fed IM startup (f_o=30 Hz). Time frequency distribution of i_{sap} current for the healthy motor.

It is important to note that the demodulation process produces a time-variant double spectrum shifting in the startup transient, which implies that all the harmonic-components from the original one-phase current are double shifted according to the instantaneous frequency ω_s. i.e. For example, the amplitude of the spectral line at $\sigma_2(t)$ (linear ramp 0 to 60 Hz) in Fig. 11 is the result of a sum of two shifted components from the original one-phase current content. $\omega_s(t)$ (linear ramp 0 to f_o=30Hz) and $h3(t)$ (linear ramp 0 to 90Hz) are shifted by the carrier (linear ramp 0 to 30 Hz) in a positive and negative side respectively. As in real IM the three-phase currents are not perfectly balacned, destructive interference does not attain its maximum value in the superposition process resulting in a spurious component located at $\sigma_2(t)$ in the t-f distribution.

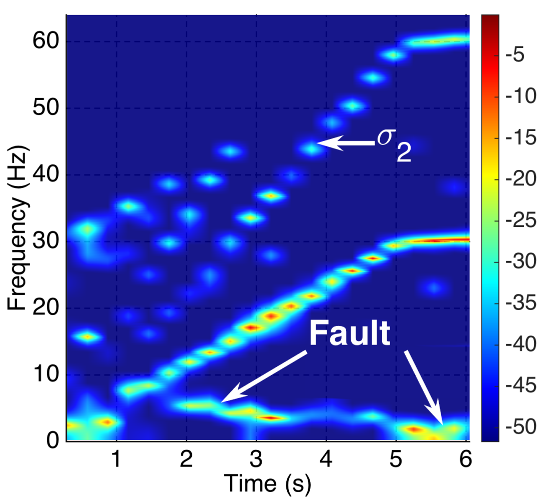

Fig. 12. Experimental result of inverter-fed IM startup (f_o=30 Hz). Time frequency distribution of i_{sap} current for the faulty motor.

It is also worth noting in Fig. 10 and Fig.12 that the energy located at $\sigma_2(t)$ increase when the bar is broken due to the asymmetries generated between current phases. Despite the presence of these components, it is possible to precisely localize the fault trajectories in Fig. 10 and Fig. 12. For the second case of study in Fig. 12 it can be noticed that the fault harmonic is very close to zero-frequency value, since $\omega_s(t)$ is small during the startup transient. However, comparing Fig. 11 and Fig.12 it is clear that the presented method can be successfully applied to IMs even in low-speed applications.

VI. Conclusions

Tracking of a new fault-harmonic product of non-uniform demodulation and superposition has been proposed for detecting BRB in IMs under large speed variation. The proposed method was successfully applied to analyze signals measured from a VSI-fed IM at different startup frequencies. Its effectiveness to track the fault-harmonic was confirmed by experimental results, proving that the technique is promising for fault diagnosis under start-up transient and steady-state since the fault-harmonic is separated and energy of the fundamental frequency is reduced. Additionally, since the fault-harmonic is a narrowband signal and a low-pass signal, the detection method can be implemented even with data acquisition systems that operates with a low sampling rate.

VII. References

[1] A. T. de Almeida, F. J. T. E. Ferreira and G. Baoming, *"Beyond Induction Motors—Technology Trends to Move Up Efficiency," IEEE Trans. Ind. App.*, vol. 50, no. 3, pp. 2103-2114, May-June 2014.

[2] A. Sapena-Bano, J. Burriel-Valencia, M. Pineda-Sanchez, R. Puche-Panadero and M. Riera-Guasp, *"The Harmonic Order Tracking Analysis Method for the Fault Diagnosis in Induction Motors Under Time-Varying Conditions," IEEE Trans. Energy Convers.*, vol. 32, no. 1, pp. 244-256, March 2017.

[3] M. Ojaghi and M. Mohammadi, *"Unified Modeling Technique for Axially Uniform and Nonuniform Eccentricity Faults in Three-Phase Squirrel Cage Induction Motors," IEEE Trans. Ind. Electron.*, vol. 65, no. 7, pp. 5292-5301, July 2018.

[4] M. Ojaghi, M. Sabouri and J. Faiz, *"Performance Analysis of Squirrel-Cage Induction Motors Under Broken Rotor Bar and Stator Inter-Turn Fault Conditions Using Analytical Modeling," IEEE Trans. Magn.*, vol. 54, no. 11, pp. 1-5, Nov. 2018.

[5] H. Henao *et al.*, "Trends in Fault Diagnosis for Electrical Machines: A Review of Diagnostic Techniques," *IEEE Ind. Electron. Mag.*, vol. 8, no. 2, pp. 31-42, June 2014.

[6] F. J. T. E. Ferreira and A. T. de Almeida, *"Reducing Energy Costs in Electric-Motor-Driven Systems: Savings Through Output Power Reduction and Energy Regeneration," IEEE Ind. Appl. Mag.*, vol. 24, no. 1, pp. 84-97, Jan.-Feb. 2018.

[7] J. Pons-Llinares, J. A. Antonino-Daviu, M. Riera-Guasp, S. Bin Lee, T. Kang and C. Yang, *"Advanced Induction Motor Rotor Fault Diagnosis Via Continuous and Discrete Time–Frequency Tools," IEEE Trans. Ind. Electron.*, vol. 62, no. 3, pp. 1791-1802, March 2015.

[8] J. Pons-Llinares, D. Morinigo-Sotelo, O. Duque-Perez, J. Antonino-Daviu and M. Perez-Alonso, "Transient detection of close components through the chirplet transform: Rotor faults in inverter-fed induction motors," in *IEEE* IECON, Dallas, TX, 2014, pp. 3386-3392.

[9] T. A. Garcia-Calva, D. Morinigo-Sotelo and R. de Jesus Romero-Troncoso, "Non-Uniform Time Resampling for Diagnosing Broken Rotor Bars in Inverter-Fed Induction Motors," *IEEE Trans. Ind. Electron.*, vol. 64, no. 3, pp. 2306-2315, March 2017.

[10] R.J. Romero-Troncoso, A. Garcia-Perez, D. Morinigo-Sotelo, O. Duque-Perez, R.A. Osornio-Rios, M.A. Ibarra-Manzano, "Rotor unbalance and broken rotor bar detection in inverter-fed induction motors at start-up and steady-state regimes by high-resolution spectral analysis", *Electr. Power Syst. Res.*, vol. 133, pp. 142-148, 2016.

[11] A. Garcia-Perez, R. J. Romero-Troncoso, D. Camarena-Martinez, R. A. Osornio-Rios and J. P. Amezquita-Sanchez, "Broken rotor bar detection in inverter-fed induction motors by time-corrected instantaneous frequency spectrogram," *in IEEE* SDEMPED, Tinos, 2017, pp. 280-285.

[12] J. Kim, S. Shin, S. B. Lee, K. N. Gyftakis, M. Drif and A. J. M. Cardoso, *"Power Spectrum-Based Detection of Induction Motor Rotor Faults for*

Immunity to False Alarms," IEEE Trans. Energy Convers., vol. 30, no. 3, pp. 1123-1132, Sept. 2015.

[13] M. Drif and A. J. M. Cardoso, *"Stator Fault Diagnostics in Squirrel Cage Three-Phase Induction Motor Drives Using the Instantaneous Active and Reactive Power Signature Analyses," IEEE Trans. Industrial Inf.,* vol. 10, no. 2, pp. 1348-1360, May 2014.

[14] F. Batista, P. C. M. Lamim Filho, R. Pederiva and V. A. D. Silva, "An Empirical Demodulation for Electrical Fault Detection in Induction Motors," *IEEE Trans. Instrum. Meas.*, vol. 65, no. 3, pp. 559-569, March 2016.

[15] Z. Hou, J. Huang, H. Liu, T. Wang and L. Zhao, "A current product signal analysis method for rotor fault diagnosis in induction motors," in *SDEMPED*, Guarda, 2015, pp. 27-32.

[16] Y. Gritli, C. Rossi, D. Casadei, F. Filippetti and G. Capolino, *"A Diagnostic Space Vector-Based Index for Rotor Electrical Fault Detection in Wound-Rotor Induction Machines Under Speed Transient," IEEE Trans. Ind. Electron.*, vol. 64, no. 5, pp. 3892-3902, May 2017.

[17] Gurmeet Singh, V.N.A. Naikan, *"Detection of half broken rotor bar fault in VFD driven induction motor drive using motor square current MUSIC analysis", Mech. Syst. and Signal Process.*, vol. 110, pp. 333-348, 2018.

[18] Y. Amirat, V. Choqueuse and M. E. H. Benbouzid, *"Wind turbines condition monitoring and fault diagnosis using generator current amplitude demodulation,"* 2010 *IEEE ENERGYCON*, Manama, 2010, pp. 310-315.

[19] Marcin Firla, Zhong-Yang Li, Nadine Martin, Christian Pachaud, Tomasz Barszcz, *"Automatic characteristic frequency association and all-sideband demodulation for the detection of a bearing fault", Mech. Syst. and Signal Process.,* vol. 80, pp. 335-348, 2016.

[20] M. Sahraoui, A. J. M. Cardoso and A. Ghoggal, *"The Use of a Modified Prony Method to Track the Broken Rotor Bar Characteristic Frequencies and Amplitudes in Three-Phase Induction Motors," IEEE Trans. Ind. Appl.,* vol. 51, no. 3, pp. 2136-2147, May-June 2015.

[21] A. Naha, A. K. Samanta, A. Routray and A. K. Deb, *"A Method for Detecting Half-Broken Rotor Bar in Lightly Loaded Induction Motors Using Current," IEEE Trans. Instrum. Meas.*, vol. 65, no. 7, pp. 1614-1625, July 2016.

[22] Y. Tanaka, *"Spectral Domain Sampling of Graph Signals," IEEE Trans. Signal Process.*, vol. 66, no. 14, pp. 3752-3767, 15 July15, 2018.

VIII. Biographies

Tomas A. Garcia-Calva (S'07) received the B.E. degree in 2014 and the M.E. (*cum laude*) degree in 2016 from the University of Guanajuato, Salamanca, Mexico, where he is currently working toward the Ph. D. in electrical engineering. He was an intern with the Universidad de Valladolid, Valladolid, Spain, and with the Universitat Politécnica de Valéncia, Valéncia, Spain, in 2016. His research interests include hardware signal processing, spectral analysis, and condition monitoring of electrical machines.

Daniel Morinigo-Sotelo (M'04) received the B.S. and Ph.D. degrees in electrical engineering from the University of Valladolid (UVA), Spain, in 1999 and 2006, respectively. He was a research collaborator on Electromagnetic Processing of Materials with the Light Alloys Division of CIDAUT Foundation since 2000 until 2015. He is currently with the Research Group on Analysis and Diagnostics of Electrical Grids and Installations (ADIRE), which belongs to the ITAP Institute UVA, and with the HSPdigital Research Group, Mexico. His current research interests include fault detection and diagnostics of induction machines, power quality, and smart grids.

Arturo Garcia-Perez (M'10) received the B.E. and M.E. degrees in electronics from the University of Guanajuato, Mexico, and the Ph.D. degree in electrical engineering from the University of Texas, Dallas, USA. He is currently an Associate Professor with the Department of Electronic Engineering, University of Guanajuato. He is a National Researcher with the Consejo Nacional de Ciencias y Tecnología. His fields of interest include digital signal processing.

David Camarena-Martinez (M'16) received the B.E. and M.E. degrees in electronics from the University of Guanajuato, Salamanca, Mexico, in 2009 and 2011, respectively, and the Ph.D. degree in mechatronics from the Autonomous University of Queretaro, Queretaro, Mexico, in 2015. He is currently a Professor with the University of Guanajuato. He is a Member of the Mexican National Research System (SNI), level 1. His research interests include hardware signal processing on field programmable gate arrays (FPGA) for applications in mechatronics.

Rene de J. Romero Troncoso (M'07–SM'12) received the Ph.D. degree in mechatronics from the Autonomous University of Queretaro, Queretaro, Mexico, in 2004. He is a National Researcher level 3 with the Mexican Council of Science and Technology, CONACYT. He is currently a Head Professor with the University of Guanajuato and an Invited Researcher with the Autonomous University of Queretaro, Mexico. He has been an advisor for more than 200 theses, an author of two books on digital systems (in Spanish), and a coauthor of more than 130 technical papers published in international journals and conferences. His fields of interest include hardware signal processing and mechatronics. Dr. Romero–Troncoso was a recipient of the 2004 Asociación Mexicana de Directivos de la Investigación Aplicada y el Desarrollo Tecnológico Nacional Award on Innovation for his work in applied mechatronics, and the 2005 IEEE ReConFig Award for his work in digital systems. He is part of the editorial board of Hindawi's International Journal of Manufacturing Engineering.